Current Biology 20, 697–702, April 27, 2010 ©2010 Elsevier Ltd All rights reserved DOI 10.1016/j.cub.2010.02.058

Report

# Motor Coordination via a Tug-of-War Mechanism Drives Bidirectional Vesicle Transport

Adam G. Hendricks,[1,3] Eran Perlson,[1,3] Jennifer L. Ross,[2,3] Harry W. Schroeder III,[1] Mariko Tokito,[1] and Erika L.F. Holzbaur[1,*]

[1]Department of Physiology and Pennsylvania Muscle Institute, University of Pennsylvania School of Medicine, Philadelphia, PA 19104-6085, USA

[2]Department of Physics, University of Massachusetts, Amherst, MA 01003, USA

## Summary

**The microtubule motors kinesin and dynein function collectively to drive vesicular transport. High-resolution tracking of vesicle motility in the cell indicates that transport is often bidirectional, characterized by frequent directional changes. However, the mechanisms coordinating the collective activities of oppositely oriented motors bound to the same cargo are not well understood. To examine motor coordination, we purified neuronal transport vesicles and analyzed their motility via automated particle tracking with nanometer resolution. The motility of purified vesicles reconstituted in vitro closely models the movement of LysoTracker-positive vesicles in primary neurons, where processive bidirectional motility is interrupted with frequent directional switches, diffusional movement, and pauses. Quantitative analysis indicates that vesicles copurify with a low number of stably bound motors: one to five dynein and one to four kinesin motors. These observations compare well to predictions from a stochastic tug-of-war model, where transport is driven by the force-dependent kinetics of teams of opposing motors in the absence of external regulation. Together, these observations indicate that vesicles move robustly with a small complement of tightly bound motors and suggest an efficient regulatory scheme for bidirectional motility where small changes in the number of engaged motors manifest in large changes in the motility of cargo.**

## Results

High-resolution tracking of vesicle movements in the cell has shown that in many instances, transport along the microtubule (MT) cytoskeleton is bidirectional (reviewed in [1]). Here, we investigated the mechanisms underlying bidirectional transport to address the questions of (1) whether opposing motors are simultaneously bound to cargos and engaged in active transport or whether motors of only one type/directionality are active at a time and (2) whether directionality is determined through external regulation (e.g., via effectors, binding partners, or posttranslational modifications) or is a result of the unregulated force-dependent kinetics of cargo-bound motors.

In order to reconstitute bidirectional transport in vitro, we isolated neuronal transport vesicles from a transgenic mouse line expressing low levels of the dynactin subunit dynamitin fused to GFP. In this line, GFP-dynamitin is efficiently incorporated into dynactin without altering the motility of the purified dynein-dynactin motor complex [2]. In neurons from these mice, GFP-labeled dynactin is localized in a punctate pattern in the cell soma and axons of neurons in situ and in culture (Figure 1A), consistent with the possible integration of the labeled protein into membrane-associated dynactin complexes.

We isolated membranous vesicles by differential centrifugation followed by flotation through a discontinuous sucrose density gradient [3]. Analysis of the purified vesicle fraction demonstrated the copurification of the MT motors dynein, kinesin-1, and kinesin-2 along with dynactin, including the GFP-labeled dynamitin subunit (Figure 1B). Thus, a complement of motor proteins remained tightly associated with the vesicles throughout the purification.

Proteins known to localize to the axonal transport compartment, such as synaptotagmin and synaptophysin, were also enriched in the isolated vesicles, as were markers for late endosomes and/or lysosomes, including LAMP-1 and Rab7. In contrast, Rab5, a marker for early endosomes, was not preferentially enriched in this vesicle preparation (Figure 1B). We used electron microscopy to examine negatively stained preparations of vesicles bound to MTs (Figure 1C). Vesicles had a mean diameter of 90.0 ± 2.9 nm (± standard error of the mean [SEM], n > 300), consistent with previously characterized axonal transport vesicles (50–150 nm) [4, 5].

Photobleaching was used to quantify the number of bound GFP-dynamitin molecules stably associated with purified vesicles. GFP-dynamitin integrates into dynactin at a ratio of 2.2 labeled subunits out of 4 total dynamitin subunits per complex [2]. Quantitative stepwise photobleaching of dispersed vesicles statically bound to the cover glass resulted in a bimodal distribution (Figure 1D; see also Figure S1A available online). The majority of vesicles (69%) were quenched in fewer than 10 steps, while most of the remaining vesicles were quenched in 10 to 20 steps. A fraction of the population was very bright (>20 bleaches); this likely correlates with vesicle aggregates observed by electron microscopy that did not bind well to MTs in motility assays and were excluded from further analysis. Given a mean of 7.6 ± 3.0 (± standard deviation [SD]) bleaching steps per dispersed vesicle, we estimate that on average, 3.5 ± 1.9 (±SD) dynactin molecules were bound to each vesicle.

The ratio of dynactin, kinesin-1, and kinesin-2 to dynein was measured by quantitative blotting of purified vesicle fractions, comparing multiple independent vesicle preparations to dilution series of purified recombinant standards (Figure 1E; Figures S1B and S1C). We measured a ratio of 1.3 ± 0.1 (±SEM, p = 0.01, n = 3 independent vesicle preparations) for dynactin to dynein, similar to the recently reported 1:1 stoichiometry of dynein to dynactin in yeast [6]. We found an average ratio of 0.16 ± 0.02 (±SEM, p = 0.01, n = 3 preparations) for kinesin-1 to dynein and a ratio of 0.63 ± 0.04 (±SEM, p = 0.004, n = 3) for kinesin-2 to dynein. Combined, quantitative western blotting and photobleaching yielded an estimate of 2.8 ± 1.6 (±SD) dynein molecules, 3.5 ± 1.9 dynactin molecules, 0.45 ± 0.27 kinesin-1 molecules, and 1.7 ± 1.0 kinesin-2 molecules

*Correspondence: holzbaur@mail.med.upenn.edu

[3]These authors contributed equally to this work

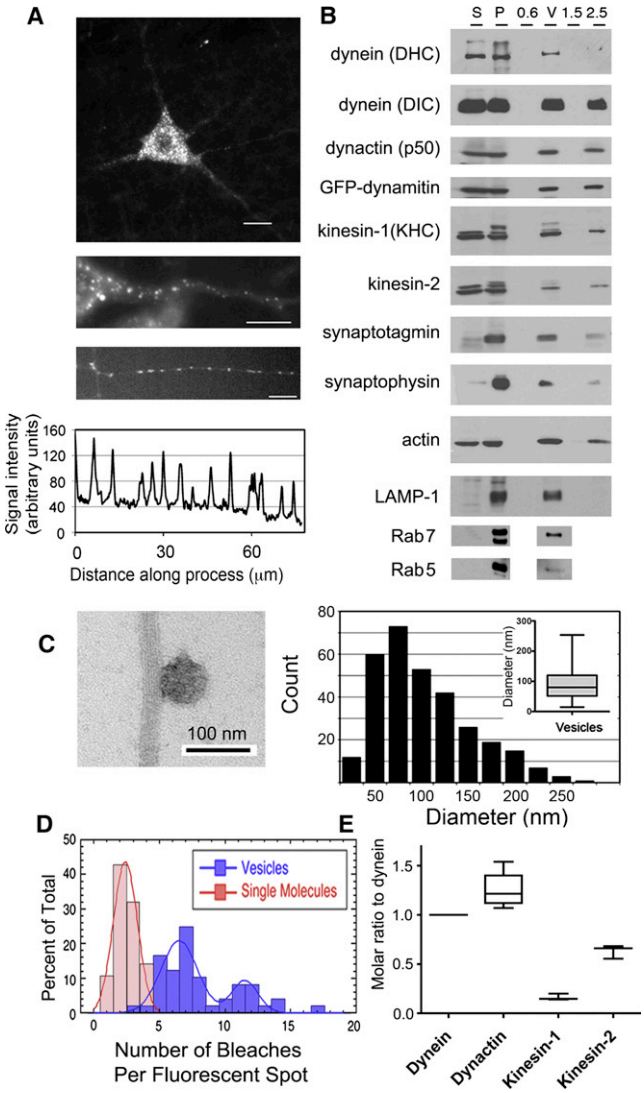


Figure 1. Microtubule Motor Proteins Dynein and Kinesin Copurify with Axonal Transport Vesicles and Drive Active Motility In Vitro

(A) Top: GFP-dynamitin is distributed in a punctate pattern throughout the cell soma and processes of motor neurons in vivo. Middle: GFP-dynamitin is localized to vesicles distributed along the axon of a motor neuron in vivo. Bottom: GFP-dynamitin is distributed to vesicles along the processes of dorsal root ganglia neurons cultured from transgenic mice expressing GFP-dynamitin. A corresponding line scan of relative fluorescent intensity along the neurite emphasizes the punctate nature of the localization.

(B) Microtubule (MT) motor proteins cytoplasmic dynein (DHC and DIC), dynactin (p50), kinesin-1 (KHC), kinesin-2, the axonal transport markers synaptotagmin and synaptophysin, and the late endosomal markers LAMP-1 and Rab7 copurify with isolated vesicles. GFP-labeled dynamitin is efficiently incorporated into the vesicle-associated dynactin complex. Fractions from the vesicle purification include initial cytosolic (S) and membrane (P) fractions from mouse brain homogenate and the 0.6 M (0.6), 0.6/1.5 M (V), 1.5 M (1.5), and 2.5 M (2.5) steps from a discontinuous sucrose gradient.

(C) Left: vesicles isolated from the 0.6/1.5 M interface were incubated with MTs and analyzed by negative-stain electron microscopy. Right: vesicles had a mean diameter of 90.0 ± 2.9 nm (±SEM, n = 311).

(D) Stepwise quantitative photobleaching of dispersed vesicles produced a bimodal distribution (blue bars). For comparison, photobleaching data for soluble purified dynein/dynactin [2] is shown (red bars).

(E) Quantitative western blotting was performed to measure vesicle-bound cytoplasmic dynein, dynactin, kinesin-1, and kinesin-2. Error bars represent SEM.

per vesicle. These measurements of the number of total cargo-bound motors are remarkably similar to previous estimates for the numbers of engaged motors driving vesicle transport in vivo, which range from one to four for kinesin and one to five for dynein [4, 7–11]. Together, these results suggest that multiple motor types are stably bound to vesicles moving along neuronal processes and that oppositely directed MT motors are bound to cargo at low, but similar, numbers.

To analyze the motility of GFP-labeled vesicles along rhodamine-labeled MTs in vitro, we used total internal reflection fluorescence (TIRF) microscopy with 16.3 nm resolution (Figure 2A). Purified vesicles showed ATP-sensitive binding to MTs (Figure 3A; Figure S3A). The slowly hydrolyzable ATP analog AMP-PNP induced the stable binding of >70% of the vesicles to MTs, consistent with the formation of a rigor bond via kinesin. Depletion of ATP also led to the formation of a rigor bond between the vesicle and the MT, presumably as a result of trapping of dynein in the strongly bound, no-nucleotide state.

Automated tracking allowed us to observe the motility of the vesicle population as a whole, as well as to categorize subsets of motility within the population. Tracking of individual vesicles moving along MTs demonstrated that vesicles frequently changed direction, with 86% of purified vesicles switching direction during an observation time of 40 s (Figure S3B). An individual vesicle may often exhibit intervals of stationary, diffusive, and processive movement. To characterize intervals of each type of bidirectional motility within runs, we used the absolute value of run length between reversals, $|L_{Rev}|$ (see Figure 2B). Characterization of motility based on $|L_{Rev}|$ is consistent with the standard definitions based on mean-squared displacement (MSD; [12]), as shown in Figure S2.

Next, we compared the movement of purified vesicles along MTs in vitro to the motility of vesicles in live cells. We labeled vesicles in primary cultures of cortical neurons with LysoTracker, which preferentially labels late endosomal/lysosomal compartments, because the purified vesicles used in this study were enriched for markers of this compartment. Again, we analyzed motility via automated tracking to obtain unbiased sampling with similar spatial and temporal resolution as our in vitro assays (Figure 2C). We found that there was a close correlation between parameters of motility observed in reconstitution assays and endogenous vesicles moving in live cells (Figure 2). Processive motility occurred with approximately equal probability in either direction for both LysoTracker-positive vesicles in live cells and purified vesicles in vitro (Figure 2E). In vitro, average velocities of processive runs were similar in either direction (Figures 2F and 2G), consistent with rates measured for soluble motor proteins in single-molecule assays [13]. LysoTracker-positive vesicles in cells and purified vesicles in vitro exhibited similar velocities (Figure 2F); furthermore, they moved with comparable average velocities in either direction along cellular processes or polarity-marked MTs, respectively (Figure 2G). Both in vitro and in cells, ~20% of the total vesicle population was stationary, whereas a large fraction displayed apparently diffusive movement, defined by short run lengths between reversals and a linear dependence of MSD on time (slope of 1 in the log-log plot) (Figure 2D; Figure S2).

To further probe the interactions of opposite-polarity motors involved in bidirectional motility, we observed the effects of inhibitory antibodies to dynein and dynactin on vesicle binding and motility. Addition of polyclonal antibodies to dynein heavy chain (pAb-DHC) or intermediate chain (pAb-DIC) reduced

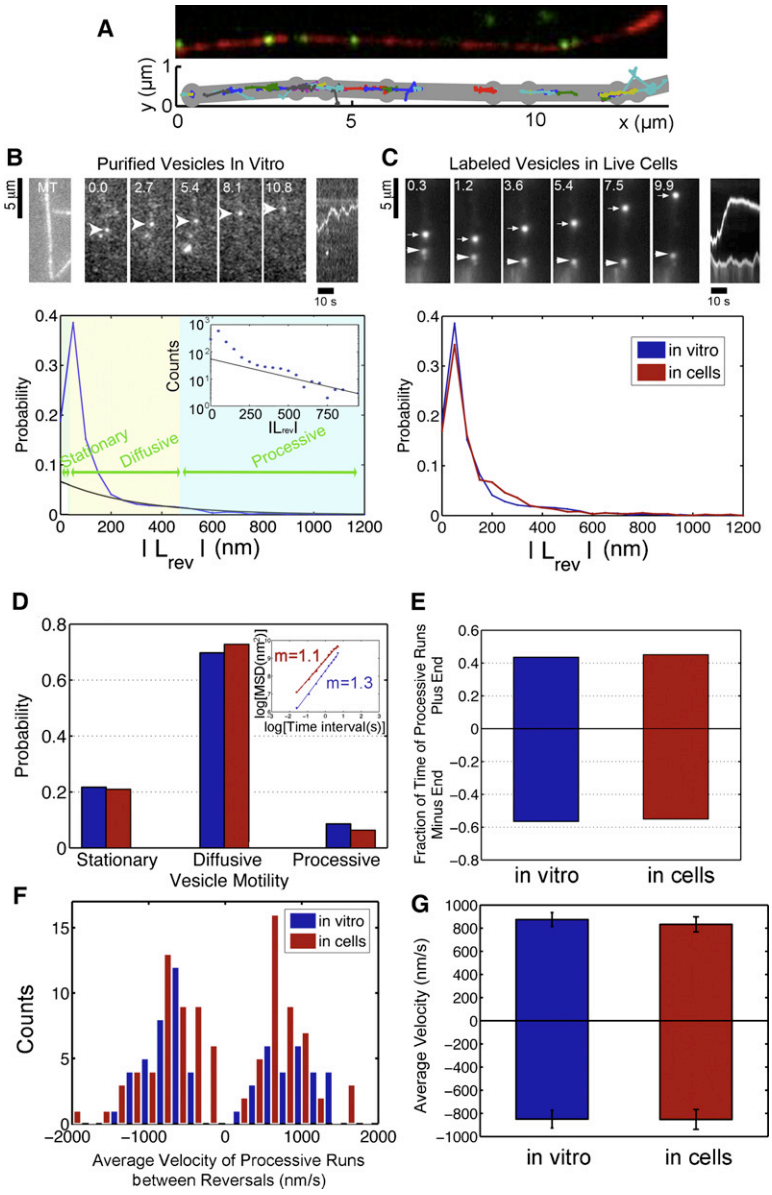


Figure 2. Bidirectional Transport of Purified Vesicles along Microtubules In Vitro Closely Models the Motility of LysoTracker-Positive Vesicles in Live Cells

(A) Automated tracking analysis of in vitro motility. Top: fluorescent vesicles (in green) moving on a polarity-marked MT (in red; plus end is bright). Bottom: custom MATLAB programs were used to automatically track the vesicles. The MT coordinates (in gray) were tracked manually in ImageJ.

(B) Top: a rhodamine-labeled MT and a time series of the movement of a GFP-labeled vesicle along the MT. A kymograph of distance moved over time is shown at the top far right. Bottom: distribution of absolute values of run lengths between reversals, $|L_{Rev}|$, from automated tracking of the vesicle population as a whole (blue curve). Intervals of motility were categorized as stationary when $|L_{Rev}| < 33$ nm (twice the standard deviation of the tracked position of an immobile vesicle attached to the coverslip). The distribution of $|L_{Rev}|$ shows a peak at <100 nm corresponding primarily to vesicle diffusion. To differentiate between diffusive and processive motility, we fit the long tail of the distribution to an exponential (black curve, characteristic decay length = 300 nm, R value = 0.8), which provides a good fit for runs > 500 nm (see inset).

(C) Top: time series and kymograph of LysoTracker-labeled vesicles in live cells showing bidirectional motility. Bottom: the distribution of $|L_{Rev}|$ for LysoTracker-positive vesicles and purified vesicles in vitro indicates similar motility.

(D) Bidirectional motility in vitro and in the cell show a similar distribution. The corresponding mean-squared displacements for all tracked vesicles (inset) are consistent.

(E) ~40% of processive motility is plus-end directed whereas ~60% is toward the minus end for purified vesicles and LysoTracker-labeled vesicles.

(F) Distribution of observed velocities for processive motility of vesicles in vitro (100 μM ATP) and in live cells.

(G) The average velocity of processive runs in the plus- and minus-end directions is similar for LysoTracker-labeled vesicles in live cells and purified vesicles in vitro. Error bars represent SEM.

vesicle binding 25% ($p < 0.05$) and 40% ($p < 0.005$), respectively, compared to controls (Figure 3B). Both pAb-DHC and a monoclonal anti-dynein antibody (mAb-DIC) increased the relative fraction of processive motility without affecting velocity (Figures S3E and S3I). In contrast, addition of pAb-DHC resulted in a change in the directional bias of processive motility, with 68% of processive motion directed toward the MT plus end in the presence of the antibody (Figure S3G). Statistical analysis of data from individual tracks indicates that this is a significant change from controls ($p < 0.0085$, $n = 43$).

To examine the role of dynactin in vesicle motility, we used a monoclonal antibody to the CAP-Gly domain of the $p150^{Glued}$ subunit of dynactin (mAb-p150) and a polyclonal antibody that binds to the extended coiled-coil domain of $p150^{Glued}$ (pAb-p150). Addition of mAb-p150 significantly decreased the binding of vesicles to MTs (~90% compared to controls, $p < 0.0001$; Figure 3C), suggesting that the CAP-Gly domain of dynactin may play a key role in mediating an initial association of the vesicle with the MT. A second inhibitory polyclonal antibody to dynactin (pAb-p150) also decreased vesicle binding to the MT ($p < 0.05$). Of the vesicles that did bind in the presence of the anti-CAP-Gly antibody (mAb-p150), there was a noticeable increase in the extent of processive motility along the MT as compared to controls (Figure S3F). MT pelleting assays indicated that this antibody effectively inhibited the direct, nucleotide-independent binding of dynactin to MTs (Figures S3K and S3L) but did not block the dynein-dynactin association (data not shown). Thus, the CAP-Gly domain of dynactin is likely to mediate some of the diffusive motion of vesicles along MTs observed in our in vitro assay. Small interfering RNA (siRNA) depletion and reconstitution experiments have shown that loss of this domain does not affect organelle distribution or rates of organelle motility in nonpolarized cells grown in culture [14, 15]. However, the CAP-Gly domain may mediate an initial interaction of vesicles with MTs [16] and therefore enhance the efficiency of vesicle transport, a possibility consistent with the observations reported here.

Several antibodies to kinesin-1 were tested, including an antibody known to inhibit kinesin-1 motility in vitro (SUK4; [17]). None of the antibodies to kinesin-1 tested had an apparent effect on vesicle binding. In contrast, an antibody to kinesin-2 (K2.4) strongly inhibited the binding of vesicles

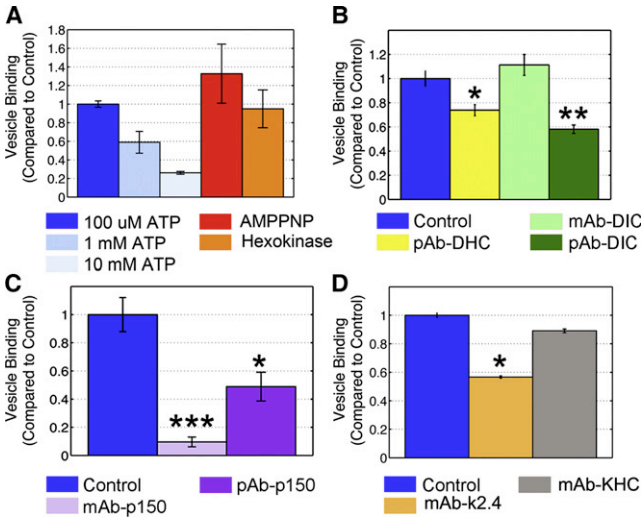


Figure 3. Binding of Vesicles to Microtubules Is Motor Driven and Dependent on Inhibitory Antibodies to Dynein, Dynactin, and Kinesin

(A) The binding of vesicles to MTs is ATP dependent. Addition of the slowly hydrolyzable ATP analog AMP-PNP increases binding, likely as a result of rigor binding of kinesin. Similarly, depletion of ATP through hexokinase increases binding, likely as a result of the rigor binding of dynein.

(B) Polyclonal antibodies (pAbs) to dynein partially inhibit vesicle binding to MTs (yellow, *$p < 0.05$; dark green, **$p < 0.005$).

(C) Vesicle binding was inhibited by addition of either mAb-p150 (light purple, ***$p < 0.0001$) or pAb-p150 (dark purple, *$p < 0.05$).

(D) Vesicle binding was inhibited by an antibody to kinesin-2 (orange, *$p < 0.05$). However, an antibody known to inhibit motility of kinesin-1 in vitro (SUK4, gray) did not have a significant effect on binding. The control for (B), (C), and (D) is binding in the presence of an anti-Myc antibody.

Error bars represent SEM.

to MTs (Figure 3D). The population of isolated vesicles described here were Rab7 positive (Figure 1B), and kinesin-2 has been identified as the primary anterograde motor for late endosomes [18–20]. These data suggest that the plus-end-directed transport of these vesicles is driven primarily by kinesin-2.

Bidirectional motility along a MT has been modeled as a stochastic tug of war [21], whereby net transport is a consequence of the force-dependent dissociation kinetics of opposing motors in the absence of external regulation. By varying the number of plus- and minus-end-directed motors or the kinetic parameters of the motors, the predicted patterns of transport exhibit a range of motility regimes, including bidirectional motility and unidirectional movement. We fit a mathematical model of bidirectional motility to our data with experimentally defined parameters for transport mediated by kinesin-1 and dynein [21] or kinesin-2 and dynein (Table S1), varying only the number of active plus- and minus-end-directed motors. The results from this modeling predict that directionality is strongly modulated by the ratio of oppositely directed motors (Figure 4A).

The predictions of the model were then compared to our experimental observations of processive motility (Figure 4B, control); the model best describes the data when transport is driven by a ratio of 7 dynein to 1 kinesin-1 motor or 3 dynein to 2 kinesin-2 motors. These predictions for the number of active motors are remarkably consistent with the experimental estimates for the ratio of total motors bound to vesicles of 6:1 for dynein:kinesin-1 and 3:2 for dynein:kinesin-2.

We also compared our experimental observations on the effect of inhibitory antibodies to dynein to theoretical predictions in which a constant number of kinesins oppose a variable number of active dynein motors (Figure 4B). The model results suggest that addition of the pAb-DHC antibody effectively decreases the number of active dynein motors. Simulated trajectories were calculated for vesicles in the absence (control) or presence of the inhibitory pAb-DHC antibody. There was a notable qualitative correlation between the observed and simulated trajectories (Figure 4C), again suggesting that the model provides a good fit to our observations.

## Discussion

Single-molecule studies on individual motors have provided significant insights into motor function (reviewed in [1, 13]). However, in the cell, multiple motor types interact collectively to drive bidirectional transport of cargos. Here, we purified endogenous vesicles along with their native complement of motors. These vesicles, in the absence of additional cytosolic regulatory factors, move bidirectionally along MTs in vitro and closely model the motility of LysoTracker-labeled vesicles in neurons.

Several models have been proposed to describe the bidirectional motion of cargo in the cell [8]. Müller et al. [21] developed a mathematical model of a stochastic tug of war in which bidirectional transport is regulated by the force-dependent kinetics of oppositely directed motors in the absence of external factors. Here we show that this model accurately describes the fast switching between plus- and minus-end-directed transport exhibited by vesicles in vitro (Figure 4). Furthermore, we find that the number of active kinesin and dynein motors predicted by the model closely correlates with estimates of the total number of bound motors as determined via photobleaching and quantitative western blotting. Thus, the model suggests that bidirectional motility directly results from the unregulated interactions of oppositely directed motor proteins simultaneously bound to the same cargo. In striking agreement with our findings, Soppina et al. [11] used optical trapping to estimate the number of motors driving the transport of *Dictyostelium* endosomes; four to eight "weak" dynein motors (~1 pN stall force) and a single "strong" kinesin motor (~5–6 pN stall force) drive each ~500–1500 nm endosome. However, in contrast to the behavior of the larger *Dictyostelium* endosomes, we did not observe "triphasic" reversals and fission events in our purified vesicles in vitro or in LysoTracker-positive organelles in live cells, suggesting that these characteristics may be specific to certain cargos.

Analysis of the motility of LysoTracker-positive organelles in live cells indicates that bidirectional motility, characterized by frequent directional switches and pauses, is a common transport mechanism for at least some types of intracellular cargo. Both in vitro and in cells, we also see that significant fractions of the total vesicle population are either paused or moving diffusionally over short distances. Tracking of vesicles in live cells also reveals that although most vesicles exhibit bidirectional motility, a subset of vesicles (~8%) move primarily unidirectionally in either the anterograde or retrograde direction (data not shown). This subset of fast, directed motility observed in the cell was not observed in vitro, suggesting that additional regulatory factors are required to reconstitute long, unidirectional runs.

Intracellular regulation may occur through several pathways. Enhanced recruitment of one motor type to a cargo

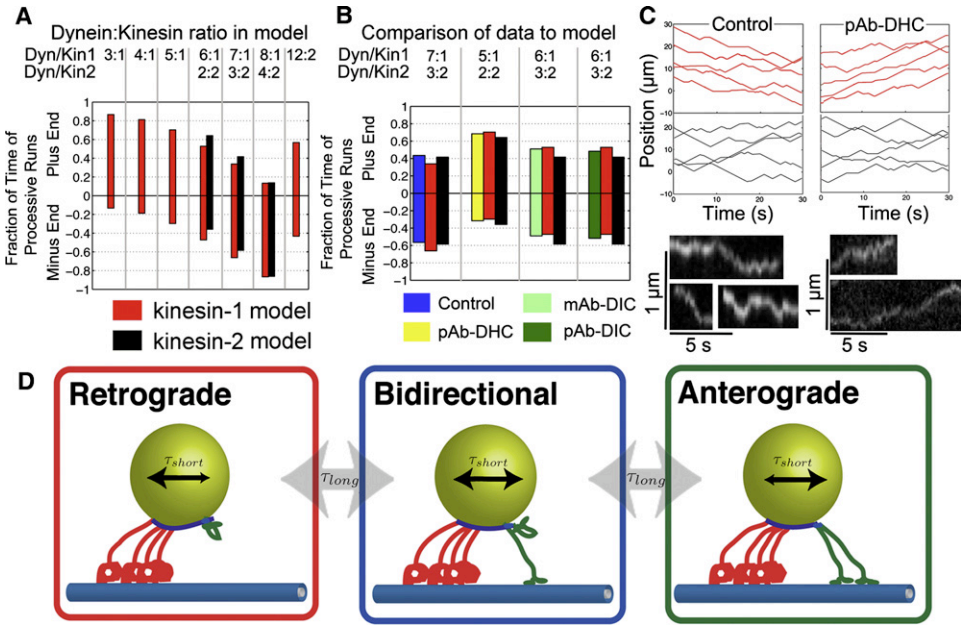


Figure 4. A Tug-of-War Model Predicts the Observed Parameters of Bidirectional Transport In Vitro

A tug-of-war model [21] was used to analyze the observed motility of neuronal transport vesicles moving bidirectionally along MTs in vitro. Model parameters were based on previous experimental observations [21, 29]. The two free parameters in the model are the number of actively engaged plus- and minus-end-directed motors.

(A) The relative fraction of time that vesicles are moving toward either the plus or minus end of the MT depends strongly on the ratio of the number of engaged plus- and minus-end-directed motors. Predictions are shown over a range of dynein:kinesin-1 and dynein:kinesin-2 ratios.

(B) Experimental data from vesicle motility along MTs are best described by a mole ratio of 7:1 dynein to kinesin-1 motors or 3:2 dynein to kinesin-2 motors. Data from vesicles treated with antibodies to DHC or DIC suggest that a fraction of the dynein is inhibited under these conditions.

(C) The Gillespie method [28] was used to generate simulated trajectories for control vesicles as well as vesicles incubated with pAb-DHC for motility driven by dynein and kinesin-1 (red) and dynein and kinesin-2 (black). Simulated trajectories are compared to kymographs of vesicle motility (excerpted from Figure S4).

(D) Regulation of bidirectional transport likely occurs at several levels. Recruitment, activation, or inhibition of motor proteins regulates the number of active motors associated with vesicular cargo. Regulation on a longer timescale ($\tau_{long}$) likely involves motor effectors. At shorter timescales ($\tau_{short}$), net directionality of movement results from a stochastic tug of war among opposing motor proteins bound to the same cargo and actively engaged with the MT.

would result in a directional bias. Alternatively, scaffolding molecules have been proposed to regulate motors on cargo. Directional switching may also be regulated at the level of motor activity, whereby the activity of the motors is stochastically modulated to affect the net direction of motion (Figure 4D). Kinesin-1 can fold into an inhibited conformation [22]; intramolecular autoinhibition through folding has also been demonstrated for other members of the kinesin superfamily [23]. Although binding to cargo was initially proposed to unfold kinesin and activate motility, recent studies indicate that activation occurs in multiple steps [24, 25], and thus even kinesin motors tightly associated with cargo may alternate between active and inactive conformations.

Unlike for kinesin, no self-regulation scheme has been demonstrated for dynein and dynactin, suggesting that only a single motor type may be actively regulated. In a "dynein-dragging model," kinesin is regulated by autoinhibition but dynein remains constitutively active. Because dynein is both less powerful and more flexible than kinesin motors and can stay associated with the MT track even in the presence of obstacles [26], dynein could potentially enhance the processivity of cargos moving in either direction. Importantly, force measurements indicate that the stall forces of both kinesin-1 (~6 pN; reviewed in [1]) and kinesin-2 (~4 pN; H.W.S., V.I. Rodionov, and Y.E. Goldman, unpublished data) are significantly stronger than the opposing force of a mammalian dynein motor (~1.1 pN; [27]). Thus, at a ratio of 1 kinesin-1 to 7 dynein motors or 2 kinesin-2 to 3 dynein motors, forces in either direction are balanced and would be predicted to result in a tug of war with approximately equal fractions of plus- and minus-ended motility such as we observed.

In the cell, regulation of bidirectional transport likely occurs at many levels (Figure 4D). At long timescales, motor recruitment and/or inhibition modulates the number of active motors, biasing the tug of war between directed retrograde and anterograde transport and bidirectional movement. At the short timescales within each motility regime, transport is driven by the subset of active motors via a stochastic tug-of-war mechanism. Accordingly, our observation that vesicles move robustly with a small complement of motors suggests an efficient regulatory scheme whereby small changes in the number of engaged motors manifest in large changes in the motility of the cargo.

### Experimental Procedures

Detailed information on methods is provided in the Supplemental Experimental Procedures. Briefly, we purified vesicles from transgenic mice expressing GFP-dynamitin [2]. Quantitative western blotting of multiple vesicle preparations was compared to purified recombinant DIC, dynamitin, kinesin-1 (KHC), or kinesin-2. Quantitative photobleaching was performed on dispersed fluorescent spots [2] corresponding to individual vesicles. Motility assays were performed with isolated vesicles and MTs polymerized

from purified tubulin via TIRF microscopy [3]. Mathematical modeling was performed with experimentally derived parameters for kinesin-1 and dynein [21] and estimated parameters for kinesin-2 (Table S1). The number of plus- and minus-end-directed motors was varied in the model, and the predicted motility and trajectories [28] were compared to observations from in vitro vesicle transport assays.

### Supplemental Information

Supplemental Information includes one table, four figures, Supplemental Experimental Procedures, and two movies and can be found with this article online at doi:10.1016/j.cub.2010.02.058.

### Acknowledgments

The authors acknowledge the scientific generosity of Y. Goldman, W. Hancock, V. Rodionov, V. Gelfand, and F. Ruhnow. E.L.F.H. was funded by National Institutes of Health (NIH) grant GM48661, J.L.R. was funded by NIH grant 1F32GM075754, H.W.S. was funded by NIH grant GM071339, and the microscope facility was funded by National Science Foundation Nanotechnology Science and Engineering Center grant DMR04-25780 and NIH grant GM087253.

Received: November 30, 2009
Revised: February 18, 2010
Accepted: February 19, 2010
Published online: April 15, 2010

### References

1. Holzbaur, E.L., and Goldman, Y.E. (2010). Coordination of molecular motors: From in vitro assays to intracellular dynamics. Curr. Opin. Cell Biol. *22*, 4–13.
2. Ross, J.L., Wallace, K., Shuman, H., Goldman, Y.E., and Holzbaur, E.L. (2006). Processive bidirectional motion of dynein-dynactin complexes in vitro. Nat. Cell Biol. *8*, 562–570.
3. Caviston, J.P., Ross, J.L., Antony, S.M., Tokito, M., and Holzbaur, E.L. (2007). Huntingtin facilitates dynein/dynactin-mediated vesicle transport. Proc. Natl. Acad. Sci. USA *104*, 10045–10050.
4. Miller, R.H., and Lasek, R.J. (1985). Cross-bridges mediate anterograde and retrograde vesicle transport along microtubules in squid axoplasm. J. Cell Biol. *101*, 2181–2193.
5. Cui, B., Wu, C., Chen, L., Ramirez, A., Bearer, E.L., Li, W.P., Mobley, W.C., and Chu, S. (2007). One at a time, live tracking of NGF axonal transport using quantum dots. Proc. Natl. Acad. Sci. USA *104*, 13666–13671.
6. Kardon, J.R., Reck-Peterson, S.L., and Vale, R.D. (2009). Regulation of the processivity and intracellular localization of Saccharomyces cerevisiae dynein by dynactin. Proc. Natl. Acad. Sci. USA *106*, 5669–5674.
7. Ashkin, A., Schütze, K., Dziedzic, J.M., Euteneuer, U., and Schliwa, M. (1990). Force generation of organelle transport measured in vivo by an infrared laser trap. Nature *348*, 346–348.
8. Gross, S.P. (2004). Hither and yon: A review of bi-directional microtubule-based transport. Phys. Biol. *1*, R1–R11.
9. Shubeita, G.T., Tran, S.L., Xu, J., Vershinin, M., Cermelli, S., Cotton, S.L., Welte, M.A., and Gross, S.P. (2008). Consequences of motor copy number on the intracellular transport of kinesin-1-driven lipid droplets. Cell *135*, 1098–1107.
10. Sims, P.A., and Xie, X.S. (2009). Probing dynein and kinesin stepping with mechanical manipulation in a living cell. ChemPhysChem *10*, 1511–1516.
11. Soppina, V., Rai, A.K., Ramaiya, A.J., Barak, P., and Mallik, R. (2009). Tug-of-war between dissimilar teams of microtubule motors regulates transport and fission of endosomes. Proc. Natl. Acad. Sci. USA *106*, 19381–19386.
12. Nelson, S.R., Ali, M.Y., Trybus, K.M., and Warshaw, D.M. (2009). Random walk of processive, quantum dot-labeled myosin Va molecules within the actin cortex of COS-7 cells. Biophys. J. *97*, 509–518.
13. Ross, J.L., Ali, M.Y., and Warshaw, D.M. (2008). Cargo transport: Molecular motors navigate a complex cytoskeleton. Curr. Opin. Cell Biol. *20*, 41–47.
14. Kim, H., Ling, S.C., Rogers, G.C., Kural, C., Selvin, P.R., Rogers, S.L., and Gelfand, V.I. (2007). Microtubule binding by dynactin is required for microtubule organization but not cargo transport. J. Cell Biol. *176*, 641–651.
15. Dixit, R., Levy, J.R., Tokito, M., Ligon, L.A., and Holzbaur, E.L. (2008). Regulation of dynactin through the differential expression of p150Glued isoforms. J. Biol. Chem. *283*, 33611–33619.
16. Vaughan, P.S., Miura, P., Henderson, M., Byrne, B., and Vaughan, K.T. (2002). A role for regulated binding of p150(Glued) to microtubule plus ends in organelle transport. J. Cell Biol. *158*, 305–319.
17. Ingold, A.L., Cohn, S.A., and Scholey, J.M. (1988). Inhibition of kinesin-driven microtubule motility by monoclonal antibodies to kinesin heavy chains. J. Cell Biol. *107*, 2657–2667.
18. Loubéry, S., Wilhelm, C., Hurbain, I., Neveu, S., Louvard, D., and Coudrier, E. (2008). Different microtubule motors move early and late endocytic compartments. Traffic *9*, 492–509.
19. Brown, C.L., Maier, K.C., Stauber, T., Ginkel, L.M., Wordeman, L., Vernos, I., and Schroer, T.A. (2005). Kinesin-2 is a motor for late endosomes and lysosomes. Traffic *6*, 1114–1124.
20. Bananis, E., Nath, S., Gordon, K., Satir, P., Stockert, R.J., Murray, J.W., and Wolkoff, A.W. (2004). Microtubule-dependent movement of late endocytic vesicles in vitro: Requirements for dynein and kinesin. Mol. Biol. Cell *15*, 3688–3697.
21. Müller, M.J., Klumpp, S., and Lipowsky, R. (2008). Tug-of-war as a cooperative mechanism for bidirectional cargo transport by molecular motors. Proc. Natl. Acad. Sci. USA *105*, 4609–4614.
22. Stock, M.F., Guerrero, J., Cobb, B., Eggers, C.T., Huang, T.G., Li, X., and Hackney, D.D. (1999). Formation of the compact confomer of kinesin requires a COOH-terminal heavy chain domain and inhibits microtubule-stimulated ATPase activity. J. Biol. Chem. *274*, 14617–14623.
23. Imanishi, M., Endres, N.F., Gennerich, A., and Vale, R.D. (2006). Autoinhibition regulates the motility of the C. elegans intraflagellar transport motor OSM-3. J. Cell Biol. *174*, 931–937.
24. Blasius, T.L., Cai, D., Jih, G.T., Toret, C.P., and Verhey, K.J. (2007). Two binding partners cooperate to activate the molecular motor kinesin-1. J. Cell Biol. *176*, 11–17.
25. Hackney, D.D., Baek, N., and Snyder, A.C. (2009). Half-site inhibition of dimeric kinesin head domains by monomeric tail domains. Biochemistry *48*, 3448–3456.
26. Dixit, R., Ross, J.L., Goldman, Y.E., and Holzbaur, E.L. (2008). Differential regulation of dynein and kinesin motor proteins by tau. Science *319*, 1086–1089.
27. Mallik, R., Carter, B.C., Lex, S.A., King, S.J., and Gross, S.P. (2004). Cytoplasmic dynein functions as a gear in response to load. Nature *427*, 649–652.
28. Gillespie, D.T. (1976). A general method for numerically simulating the stochastic time evolution of coupled chemical reactions. J. Comput. Phys. *22*, 403–434.
29. Muthukrishnan, G., Zhang, Y., Shastry, S., and Hancock, W.O. (2009). The processivity of kinesin-2 motors suggests diminished front-head gating. Curr. Biol. *19*, 442–447.